ATOMISTIC STUDIES OF PROPERTIES OF HELIUM IN BCC IRON -

David Stewart, Yuri Osetskiy, and Roger Stoller (Oak Ridge National Laboratory)

OBJECTIVE

The objective of this work is to use molecular dynamics techniques to increase understanding of the behavior of transmutation-produced helium in reduced-activation ferritic/martensitic steels that are candidate materials for fusion reactors. As there is no suitable iron-carbon-helium interatomic potential, simulations are performed using helium in pure iron.

SUMMARY

Helium created by transmutations plays an important role in the response of reduced-activation ferritic/martensitic (RAFM) steels to neutron radiation damage. We have performed extensive atomistic simulations using the ORNL 3-body Fe–He interatomic potential combined with three interatomic potentials for the iron matrix. Interstitial helium is very mobile and coalesces to form interstitial clusters, with some mobility of small clusters. When an interstitial He cluster reaches sufficient size, it punches out an Fe interstitial, creating an immobile helium–vacancy cluster. If more helium atoms join it, more Fe interstitials can be created, and the He–V defect is a nascent bubble. These mechanisms are investigated in simulations that examine the nucleation of He defects. Mobile interstitial He clusters and helium bubbles 1 to 6 nm diameter are also simulated separately. Results are compared based on temperature and interatomic potentials used.

PROGRESS AND STATUS

1. Introduction

Reduced activation ferritic/martensitic steels are a candidate material for use in fusion reactors [1]. The presence of transmutation-created helium plays an important role in the microstructural evolution of these steels under neutron irradiation. Kinetic models demonstrate that the growth, migration and coalescence behavior of helium defects is very sensitive to the properties of individual He interstitials and helium–vacancy clusters [2].

In a recent paper [3], we presented a detailed comparison of the behavior of He in Fe as described by the ORNL three-body potential [4–6] with that predicted by two pair potentials found in literature [7,8]. Here, we extend that work in three ways. Firstly, we simulate helium clustering over a substantially longer physical time frame. Secondly, we investigate the diffusion behavior of interstitial helium clusters as described by the different potentials. Thirdly, we simulate helium bubbles of diameter up to 6nm with different helium-to-vacancy (He/V) content over a wide temperature range.

2. Simulation Method

The NVE molecular dynamics simulation methods used in this paper are described in detail in [3]. Three different types of simulations were used here to investigate different phenomena.

Nucleation, growth and coalescence of interstitial He clusters and subsequent formation of helium–vacancy clusters and Fe interstitials were simulated by annealing a system containing a certain population of single interstitial He atoms initially homogenously distributed in BCC iron matrix. Here we describe results for 125 helium atoms in a BCC crystal containing 59,582 Fe atoms, which corresponds to the mean He concentration of 2089 appm. Annealing at several temperatures in the range from 200 to 1200K was simulated for times up to 12_ns. The Ackland Fe potential [9] was used in combination with the ORNL Fe–He potential.

Diffusion of helium interstitial clusters was modeled in a 10×10×10 box containing 2000 Fe matrix atoms. Interstitial defects of 1 to 6 helium atoms were simulated over the temperature range 250 to 1000K. Diffusion coefficients of He interstitial defects were estimated using the technique described earlier [3, 10].

A relatively long simulation time, up to 30ns, has allowed us to estimate the diffusion coefficients with a high accuracy. Typically the standard error is so small that the error bar is hidden behind the symbol on the corresponding graphs. Three potentials for the Fe matrix [9,11,12] and three Fe–He potentials [4–8] were used in this study.

The He–V defects nucleated in the coalescence simulation described above are nascent bubbles. We investigated the properties of larger bubbles, from 1 to 6nm, in larger simulated crystals, up to 432,000 Fe atoms. First a void of the corresponding size was created and then a certain number of He atoms was homogenously distributed inside. The system was then annealed for over 1ns to obtain an equilibrium state. Voids from 1 to 6 nm contain from 59 to 9577 vacancies and we simulated He-to-vacancy ratios: He/V = 0 to 0.6 in the temperature range from 100 to 900K. During this simulation we monitored the He distribution inside the bubble, the effective bubble size (radius), the He pressure inside bubbles and the total pressure in the simulated system. In these simulations we used the Ackland iron [9], the ORNL He–Fe [4–6], and the Aziz [13] helium potentials.

3. Results

3.1. Coalescence

In this study we investigated the fate of single interstitial He atoms subjected to annealing at different temperatures. The set of phenomena observed includes diffusion of He atoms and interactions in which interstitial He clusters are formed. Being small, these clusters are also mobile and can coalesce forming larger clusters. Depending on the temperature these larger clusters can change their structure from interstitial He clusters to He–vacancy clusters pressing out iron interstitial atoms. The resulting He-vacancy cluster is immobile. Further interaction with mobile interstitial He clusters leads to the formation of additional vacancy–SIA pairs, increasing the size of immobile He–vacancy clusters (growth) and the number of iron SIAs in the system.

Figure 1 shows the number of Frenkel pairs created as a function of time at different temperatures. At 200K, the helium slowly and inexorably coalesced until it formed interstitial clusters too big to be mobile. Due to the slow diffusion and the inability of even a di-helium pair to dissociate, a high density of clusters formed, each containing only 2 to 8 He atoms. After 12.9ns a cluster of size 10 formed, which created a Frenkel pair within 20ps.

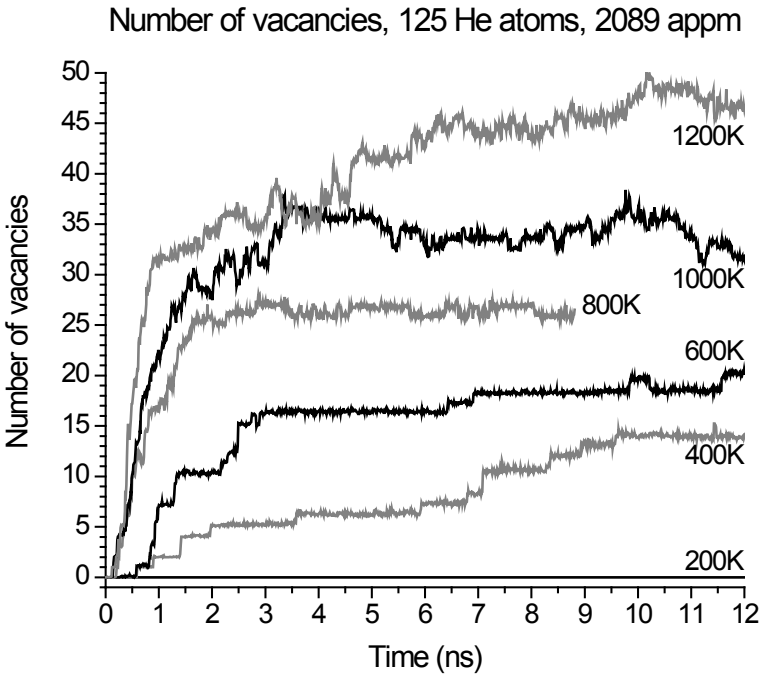

Figure 1. Vacancy production due to the formation of He–V defects for different temperature simulations.

At 400K, the helium was more able to form large clusters, and started creating Frenkel pairs when they reached 9 or more He atoms. One pair was created by a size 7 cluster. 15 Frenkel pairs were created gradually over the entire simulation. All SIAs except one remained trapped by the He–V defect that had created them.

At 600K, the number of He atoms in a cluster required to create a Frenkel pair ranged from 7 to 11. In one case a cluster of 5 created a Frenkel pair, but it recombined 0.7ns later. Defect creation proceeded more rapidly at this temperature, and most (16 of 19) Frenkel pairs were created in the first 3ns. Most SIAs remained pinned to the He–V defect that had created them.

At 800K, coalescence proceeded even faster. Frenkel pair creation, which happened in clusters of 6 or more heliums, saturated at about 25 after 2ns. After 3ns, all helium atoms were part of a He–V defect. The ejected SIAs escaped from the three single vacancy He–V defects and were captured by larger (up to 6 vacancy) ones.

At 1000K, coalescence proceeded faster still. Frenkel pair creation, which happened in clusters of 6 or more heliums, reached 30 in the first 2ns and then slowly increased further. After 3ns, all helium atoms were part of a He–V defect. Some ejected SIAs escaped from the smallest (2 vacancy) He–V defects and were captured by the larger (up to 8 vacancy) ones.
At 1200K, about 30 Frenkel pairs were created in the first nanosecond and about 15 more in the rest of the simulation. At 2.25ns, all helium atoms were part of a He–V defect, but later some helium atoms escaped from the single vacancy He–V defects and were captured by other defects. Ejected SIAs escaped from the 1 and 2 vacancy He–V defects and were captured by the larger (up to 9 vacancy) ones.

3.2. Cluster Diffusion

The study described above demonstrated the formation of mobile interstitial He clusters and we therefore investigated the mobility such clusters in this work. Depending on the number of He interstitials in the cluster and the ambient temperature three different types of behavior were observed:

- The interstitial cluster remained intact and moved as a whole. This was observed for smaller clusters at lower temperatures. In this case we could measure mobility via estimation of their diffusion coefficient.
- The interstitial cluster broke up/dissociated into smaller clusters and/or He interstitial atoms, which diffused away from each other.
- The interstitial cluster created a Frenkel pair, resulting in an SIA and an immobile helium–vacancy defect.

The second and third types of behavior were favored for larger clusters and at higher temperatures.

The cluster diffusion rate is considered to be the diffusion rate of the centre of mass of the He atoms. An Arrhenius plot of the rates is shown in Fig. 2. When a cluster remains intact, the diffusion rate is calculated using the entire simulation, and shown as a solid symbol in Fig. 2. In the cases when a cluster dissociates or ejects an SIA after a certain length of time, the diffusion coefficient is calculated from the simulation up to that point, and is shown as an empty symbol in Fig. 2.

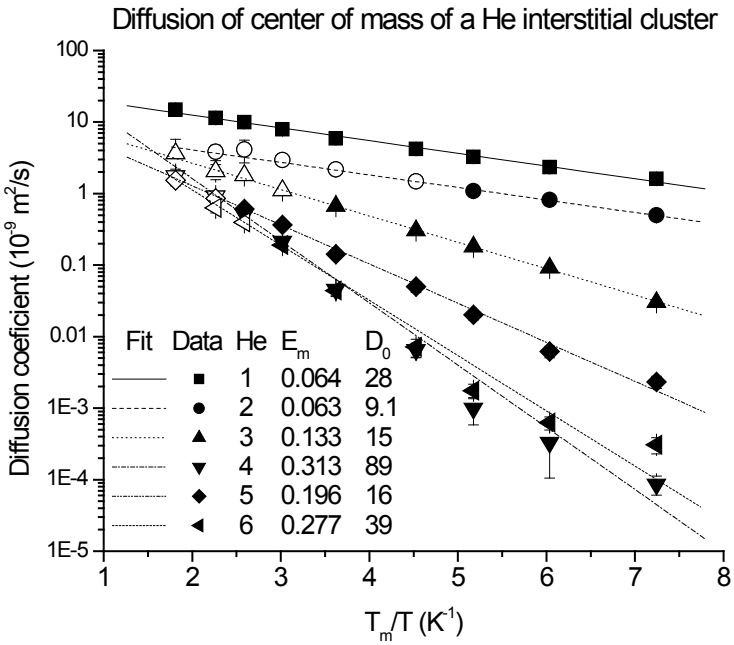

Figure 2. Arrhenius plot for diffusion of helium interstitial clusters using Ackland97 and ORNL potentials. Open symbols present treatment of He interstitial clusters diffusion before either their dissociation or formation of He–vacancy clusters and emitting iron SIAs.

Arrhenius fits to the data were done for several different combinations of matrix and He–Fe potentials, and the resulting energy barriers are plotted in Fig. 3.

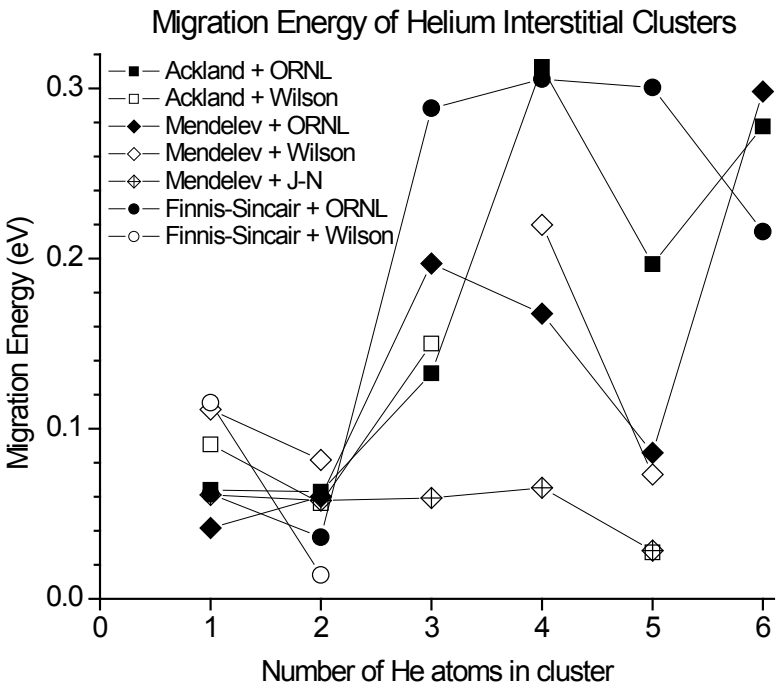

Figure 3. Cluster migration energies calculated using different interatomic potentials.

The test matrix for this measurement was 3 He–Fe potentials times 3 Fe matrix potentials times 6 He

interstitial cluster sizes times 9 different temperatures. The Juslin–Nordlund He–Fe potential [8] with Ackland [9] or Finnis–Sinclair [11] predicts that all clusters will dissociate into individual interstitial helium atoms, so there are no cluster diffusion rates for these combinations. The Mendelev matrix [12] with the Juslin–Nordlund potential showed consistently low barriers compared to the other combinations.

The Ackland matrix potential with the ORNL He–Fe potential [4–6] showed almost identical barriers of about 0.06eV for a single He and the He_2 pair. He_3 had the next lowest barrier followed by He_5. He_4 and He_6 had the highest barriers of about 0.3eV.

The Mendelev matrix with the ORNL He–Fe potential showed different behavior. The barrier for a single He was only 0.04eV and for He_2 remained at 0.06eV. The next lowest was He_5 with a barrier of only 0.09eV. He_3 and He_4 showed very similar diffusion rates and barriers of about 0.18eV. The highest barrier was He_6 with 0.3eV.

With the Finnis–Sinclair matrix and the ORNL He–Fe potential, the He_2 cluster had a lower barrier than a single He. Clusters of size 3, 4 and 5 showed very similar diffusion rates and barriers of about 0.3eV, while He_6 had a barrier closer to 0.2eV.

The Ackland matrix potential with the Wilson He–Fe potential [7] also showed the He_2 cluster with a lower barrier than a single He. Surprisingly, the He_5 cluster had an even lower barrier of only 0.03eV, based on simulations below 400K. At 400K and higher, it ejects an SIA too quickly to calculate a diffusion rate. The He_3 cluster shows very strange behavior, repeatedly ejecting an SIA and recombining with it. This suggests that the two states have similar energy. The ability of the SIA to recombine may be somewhat an artifact of the simulation, since it has periodic boundary conditions and a small size. The He_4 cluster remained intact for a long time, especially at low temperatures, but would eject an SIA rather than move. At all temperatures, the He_6 cluster ejected an SIA too quickly to calculate a diffusion rate.

The Mendelev matrix potential with the Wilson He–Fe potential again shows decreasing barriers from the single He to the He_2 cluster to the He_5 cluster. The He_4 cluster showed very slow diffusion—the barrier was 0.2eV, but it had an extremely low pre-exponential factor. The He_5 cluster showed a 2-process behavior: fast diffusion along a ⟨111⟩ direction with occasional direction changes. This suggests that there are 2 energy barriers, one for the ⟨111⟩ movement and one for the rotation. However the analysis procedure used in this work looks at the movement as a whole and generates a single (effective) diffusion coefficient. Above about 400K, He_4 and He_5 ejected an SIA too quickly the gather diffusion data. At all temperatures, the He_3 and He_6 clusters immediately ejected an SIA.

3.3 Helium bubbles

Figure 4 (visualized using the PyMol software [14]) shows a cross-section of a 4nm (2741 vacancies) bubble with He/V = 0.5. It was discovered that the helium atoms stand off a small distance from the surface iron atoms, leading to the gap visible in Figure 4. The gap was large enough that in these simulations the He atoms rarely come close enough to an iron atom to invoke the 3-body component of the ORNL Fe–He potential (range 2.2Å), so their interactions are effectively described by the pair part of the potential.

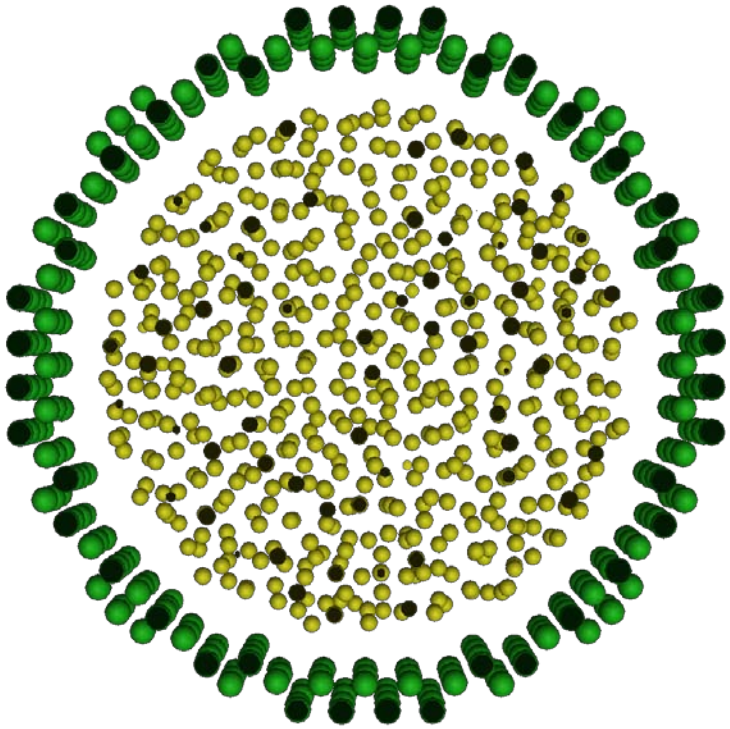

Figure 4. Cross-section from a simulation of a 4nm 0.5He/V bubble at 100K, green spheres are iron are and yellow spheres are helium atoms. Atoms cut by the cross-section plane are shown partly black.

Figure 5 shows the radial density function of an equilibrium 2nm bubble with a He/V = 0.49 at 300K. The red circles show the iron atoms that make up the surface of the bubble, while the blue squares represent the density of helium atoms in the space, averaged over a 1ns simulation. The helium density oscillates enough to suggest a shell structure to the arrangement of atoms, but not enough to suggest solid helium. This agrees with [15] prediction that the helium in the bubble would not be solid. The dotted line in the figure, an approximation to a uniform distribution, shows that the actual helium density (1.04) is just over double the nominal density (0.49). The helium occupies a sphere of radius 7.7Å (just under half the volume of the void), and the radial gap is approximately 2.2Å.

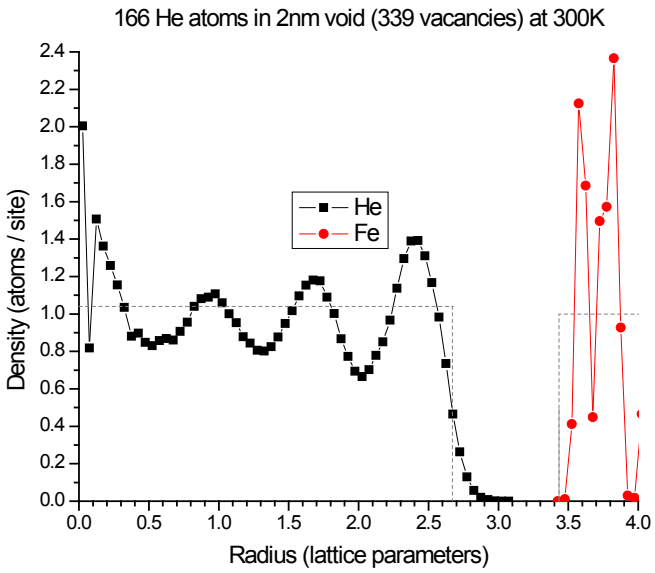

Figure 5. Radial distribution function of a 2nm equilibrium bubble at 300K.

In a void, the surface matrix atoms relax inwards slightly, reducing the volume of the void. At higher temperatures, they move in more due to the thermal expansion of the iron. Adding helium to the void pushes the atoms outwards, increasing the volume again. The more helium added, the further the bubble expands. There is a point where the forces balance and the bubble is neither expanded nor contracted; the surface atoms are at the same place as they would be in a perfect lattice. We use this point as our condition for equilibrium. The equilibrium He/V ratio is temperature and size dependant. In general, the equilibrium He/V ratio is lower for higher temperatures and larger bubbles.

Figure 6 shows the dilation of a 2nm diameter bubble as a function of He/V ratio for different temperatures. The equilibrium ratio for each temperature can be determined by where it crosses the horizontal zero line. At 2nm, the curves for the different temperatures are close together and the equilibrium He/V ratios lie in the range 0.4–0.55; for larger bubbles, the curves spread out more (not shown).

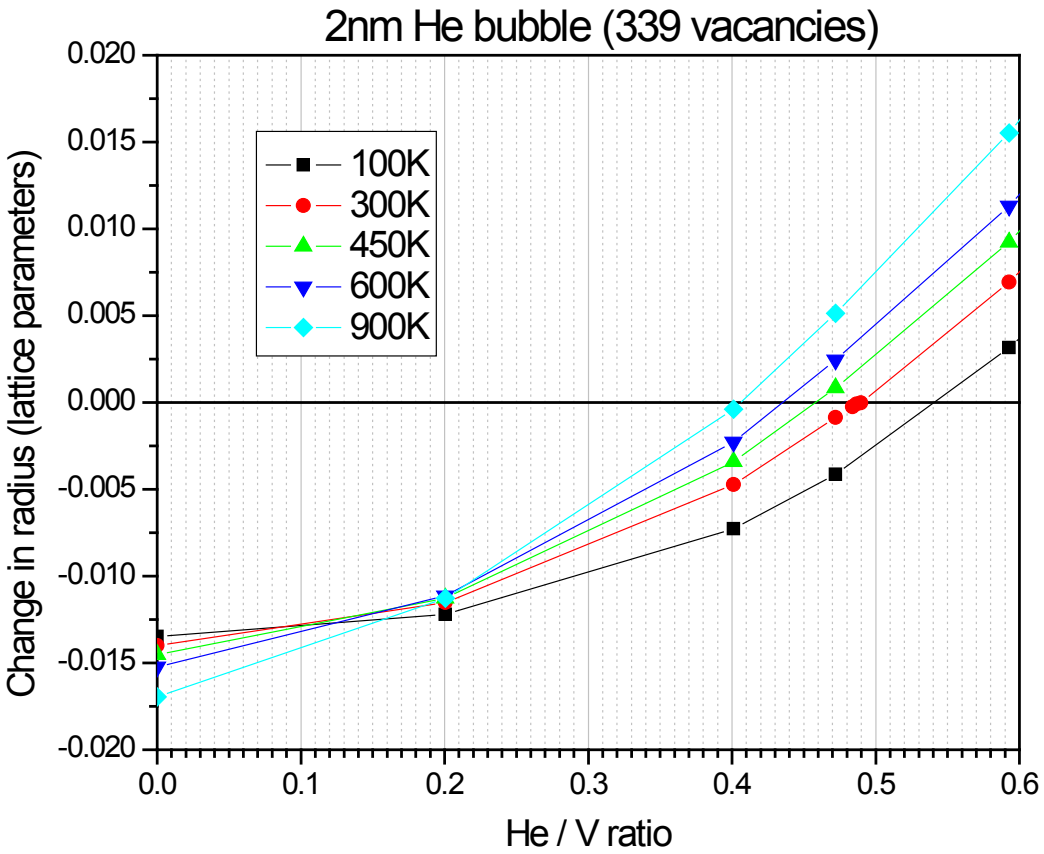

Figure 6. Dilation of 2nm bubbles as a function of He/V ratio at different temperatures.

Figure 7 shows the dilation of different sized bubbles as a function of He/V ratio at 300K. The He/V ratio at equilibrium initially decreases as the bubble size increases, but the incremental change is reduced for smaller bubbles. There is little change in the equilibrium ratio between a 2 and 1.5 nm bubble, and the ratio increases for smaller sizes as shown by the curve for the 1nm bubble. Since the equilibrium pressure (which increases as ratio increases) is expected to follow a $2\gamma/r$ relationship (where γ is the surface energy and r is the bubble radius), the reduction in ratio with increasing size for the 2, 4 and 6nm bubbles is expected. The bubble volume is defined by the position of the surface iron atoms, but the volume actually occupied by helium is defined by the He atom positions, and is substantially smaller. The smaller the bubble gets, the greater fraction of the bubble volume is in the He-free gap and the less is occupied by helium. In the 1nm bubbles the helium occupies less than 30% of the volume, which leads to the reduction in the equilibrium ratio.

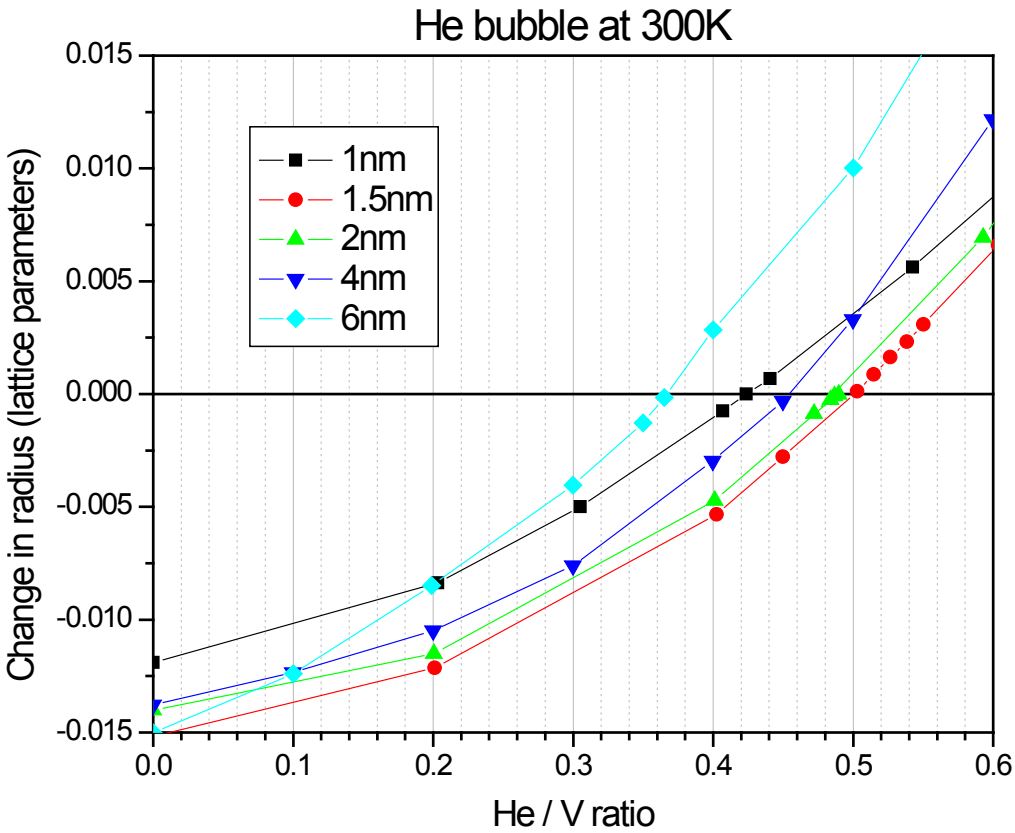

Figure .7 Dilation of different size bubbles as a function of He/V ratio at 300K.

4. Discussion and Conclusions

4.1. Coalescence

Simulations investigating the nucleation of nascent helium bubbles from interstitial helium atoms were carried out using the Ackland iron and ORNL He–Fe potentials. He interstitial cluster growth, coalescence and Frenkel pair creation were almost negligible at 200K but prevalent at all higher temperatures. The temperature affected not just the rate but also the nature of the defect creation process.

The higher the temperature, the faster He atoms and clusters diffuse, which makes coalescence occur faster. This is balanced by higher temperatures leading to small clusters being broken up, delaying the creation of larger, stable clusters. The result is that that the cluster size distribution is temperature dependant: higher temperatures lead to fewer but larger clusters. Higher temperatures also increase the number of Frenkel pairs likely to be emitted from a larger He–V cluster.

4.2 Cluster Diffusion

Diffusion rates for clusters of 1 to 6 interstitial helium atoms were calculated for several combinations of potentials. Three combinations, Ackland + ORNL, Finnis–Sinclair + ORNL and Mendelev + Juslin–Nordlund reproduced the DFT result [16] of 0.06 eV for the migration of a single He interstitial. In general, larger clusters were found to diffuse slower, however there were significant differences between the potentials. He_2 clusters tended to have a similar or lower energy barrier than single interstitial helium atoms but still diffuse slower due to a lower pre-exponential factor. The ORNL and Wilson potentials show significantly higher barriers for He_3 and larger. The J–N potential shows barriers of about 0.06eV for

clusters of 1 to 4 interstitials, with the pre-exponential factor decreasing with increasing cluster size. He_5 was found to have a (usually substantially) lower migration barrier than He_4 with all combinations of potentials used. A possible explanation is that the tetrahedral arrangement of He_4 is much more stable due to its high symmetry that matches the symmetry of the Fe matrix. He_5 configurations are far less symmetrical and, in some potentials, allow for rapid 1D diffusion.

4.3 Bubbles

1, 1.5, 2, 4 and 6nm diameter bubbles have been simulated. In a void, the surface matrix atoms relax inwards; the addition of helium atoms pushes them back outwards. The balance point (i.e. zero total dilation) defines an equilibrium condition.

The equilibrium He/V ratio is size dependent, with a maximum when the bubble diameter is close to 1.5nm. Larger bubbles have a smaller ratio because the pressure is lower, while smaller bubbles have a smaller ratio because the space available for helium decreases rapidly due to the increasing fraction of the volume accounted for by the He-free gap. The equilibrium He/V ratio also decreases as temperature increases, so bubbles formed under high temperature irradiation may be out of equilibrium during room temperature experiments.

This paper provides a brief review of the general phenomena and mechanisms observed in extensive simulations of He atom behavior inside an Fe matrix. More detailed descriptions of the mechanisms observed and their quantification will be presented in separate publications.

Acknowledgement

Research sponsored by the Office of Fusion Energy Sciences (DMS) and the Division of Materials Sciences and Engineering (YNO, RES), U.S. Department of Energy, under contract DE-AC05-00OR22725 with UT-Battelle, LLC.

References

[1] S. J. Zinkle, Physics of Plamas, 12 (2005) p. 058101.
[2] S. I. Golubov, R. E. Stoller, S. J. Zinkle, and A. M. Ovcharenko, J. Nucl. Mater. 361 (2007) p. 149.
[3] D. M. Stewart, Y. N. Osetsky, R. E. Stoller, S. I. Golubov, T. Seletskaia1, P. J. Kamenski, accepted for publication in Philos. Mag. (2009).
[4] T. Seletskaia, Y. N. Osetsky, R. E. Stoller, and G. M. Stocks, J. Nucl. Mater. 351 (2006) p. 109
[5] T. Seletskaia, Y. N. Osetsky, R. E. Stoller, and G. M. Stocks, J. Nucl. Mater.367 (2007) p. 355.
[6] R. E. Stoller, S. I. Golubov, P. J. Kamenski, T. Seletskaia, and Yu. N. Osetsky, "Implementation of A New Fe–He Three-body Interatomic Potential for Molecular Dynamics Simulations," accepted for publication in Philos. Mag. (2009).
[7] W. Wilson and R. Johnson, Rare Gases in Metals, Interatomic Potentials and Simulation of Lattice Defects, Battelle Institute Materials Science Colloquia, 1972, 375–390 (1972).
[8] N. Juslin and K. Nordlund, J. Nucl. Mater. 382 (2008) p. 143.
[9] G. J. Ackland, D. J. Bacon, A. F. Calder, and T. Harry, Philos. Mag. A 75 (1997) p. 713.
[10] Yu. N. Osetsky, Defect and Diffusion Forum 188–190 (2001) p. 71.
[11] M. W. Finnis and J. E. Sinclair, Philos. Mag. A 50 (1984) p. 45.
[12] M. I. Mendelev, S. Han, D. J. Srolovitz, G. J. Ackland, D. Y. Sun, and M. Asta, Philos. Mag. 83 (2003) p. 3977.
[13] R. Aziz, A. Janzen, and M. Moldover, Phys. Rev. Lett. 74 (1995), pp. 1586–1589.
[14] W. L. DeLano, “The PyMol molecular graphic system,” DeLano Scientific LLC, San Carlos, Ca, USA. http://www.pymol.org.
[15] S. M. H. Haghighat, G. Lucas and R. Schäublin, Europhysics Letters 85 (2009) p, 60008
[16] C.C. Fu and F. Willaime, Phys. Rev. B 72 (2005) p. 064117.